

Evidence for Diurnal Period Kelvin Waves in the Martian Atmosphere from Mars Global Surveyor TES Data

R. John Wilson

Geophysical Fluid Dynamics Laboratory/NOAA, Princeton University, Princeton, New Jersey

Abstract. Midlevel (~25 km) atmospheric temperatures derived from Mars Global Surveyor (MGS) Thermal Emission Spectrometer (TES) spectra indicate the presence of stationary waves and thermal tides. Stationary waves are prominent at middle to high latitudes where westerly zonal flow is indicated by the meridional temperature gradient. Longitudinal variability within 30°S to 30°N is dominated by topographically-forced nonmigrating thermal tides that have westward and eastward propagating components. The MGS mapping data are available at two fixed local times so that it is not possible to distinguish between these components or isolate the sun-synchronous tide. A comparison with Mars general circulation model (MGCM) simulations suggests that the observed wave patterns are consistent with the presence of eastward propagating, diurnal period Kelvin waves with zonal wavenumbers one and two. These waves can propagate to great heights and may account for observed zonal variations in thermospheric density.

1. Introduction

The martian surface has large amplitude, planetary scale variations in topography, surface thermal inertia and albedo that can give rise to significant wave activity. The Mars Global Surveyor (MGS) Thermal Emission Spectrometer (TES) is providing atmospheric temperatures with unprecedented latitude and longitude coverage suitable for characterizing the atmospheric response to boundary forcing. The present focus is on stationary waves and thermal tides. Thermal tides are planetary waves with periods that are harmonics of the solar day. The tides include westward propagating, migrating (sun-synchronous) waves driven in response to solar heating and additional nonmigrating waves resulting from zonal variations in the thermotidal forcing [Zurek, 1976; Wilson and Hamilton, 1996, hereafter WH96; Forbes and Hagan, 2000]. Banfield *et al.* [2000] previously identified stationary waves and thermal tides at southern latitudes (poleward of 30°S) using retrieved TES temperatures from the first MGS aerobraking and science phasing orbits when good local solar time coverage was available. The MGS mapping orbits provide data at two fixed local times (2 am and 2 pm) so that the observed thermal tide is aliased by the limited time coverage. We employ a Mars global circulation model (MGCM), which is able to reasonably reproduce the observed longitudinal temperature variations, to provide additional insight into the behavior of the tidal response by enabling the decomposition of simulated temperature fields into stationary waves and eastward and westward propagating tides.

2. Nonmigrating Thermal Tides

The longitude-time dependence of stationary waves and

thermal tides may be represented as:

$$T(\lambda, t_{LT}) \sim \sum T_{s,\sigma} \cos[(s-\sigma)\lambda + \sigma t_{LT} - \delta_{s,\sigma}] \quad (1)$$

where s is the zonal wavenumber, λ is east longitude, σ is the temporal harmonic ($\sigma=1$ for the diurnal tide), t_{LT} is the local solar time, and $\delta_{s,\sigma}$ is the phase. The relation between universal and local solar time is given by $t = t_{LT} - \lambda$. Stationary waves are associated with $\sigma=0$, tides with $s > 0$ ($s < 0$) propagate westward (eastward), and zonally-symmetric tides have $s=0$. The migrating tides ($s=\sigma$) are independent of longitude in the sun-synchronous reference frame. The presence of zonal wave m modulation in the tidal forcing results in the migrating tide ($s=\sigma$) being scattered into modes with wavenumbers $\sigma-m$ and $\sigma+m$. These waves each contribute to a wave m variation when viewed in a fixed local time reference [Forbes and Hagan, 2000]. Thus, an $m=2$ modulation of the diurnal period migrating tide yields westward ($T_{3,1}$) and eastward propagating ($T_{-1,1}$) diurnal period components that contribute to a wave 2 variation in temperature. There will also be contributions from higher temporal harmonics ($T_{0,2}$, $T_{4,2}$, $T_{1,3}$, $T_{5,3}$, ... such that $s - \sigma = \pm 2$) to the observed wave 2 variation.

The latitudinal and vertical structure of the atmospheric temperature response will depend on both the structure of the forcing and on the efficiency of the atmospheric response to a given forcing. In the framework of classical tide theory, the westward propagating diurnal waves ($s=1, 2, \dots$) may be represented by a sequence of equatorially confined, vertically propagating waves and vertically trapped waves in the extratropics [Chapman and Lindzen, 1970]. The tropical waves have relatively short vertical wavelengths (less than ~ 33 km). Thermal forcing generally projects onto a set of these modes, leading to a relatively complex thermal response.

The most prominent components of the eastward propagating, diurnal period response are the diurnal Kelvin waves (DK1, DK2, ... corresponding to $s=-1, -2, \dots$) which are meridionally symmetric and broad solutions of the Laplace Tidal Equation [Chapman and Lindzen, 1970]. DK1 has a vertical structure that closely corresponds to the equivalent barotropic Lamb wave and may be resonantly enhanced [Zurek, 1988; WH96]. DK2 and DK3 are vertically propagating modes with wavelengths of roughly 90 and 50 km, respectively, and have amplitudes that increase exponentially with height. Long vertical wavelengths render these Kelvin waves less susceptible to thermal dissipation so that they may be prominent in the upper atmosphere of Mars [Conrath, 1976; Forbes and Hagan, 2000]. The presence of DK1 has been inferred from Viking lander surface pressure data and has been shown to be forced by dynamical effects induced by topography [WH96].

3. MGS TES Observations

We have synthesized an atmospheric temperature by convolving TES spectra with the $15 \mu\text{m}$ spectral response function from the Viking Infrared Thermal Mapper (IRTM) instrument [Wilson and Richardson, 2000]. The resulting temperature, T_{15} , represents a depth-weighted layer of atmosphere centered at roughly 0.5 mb or 25 km. Due to significant differences in vertical wavelengths, the relative contributions of eastward and westward propagating compo-

nents to the observed tropical tide will depend on the vertical weighting implicit in the constructed temperature. The use of the IRTM weighting function allows a consistent comparison of observed and simulated temperatures. Figure 1 shows the morning (2 am) and afternoon (2 pm) T_{15} fields for the $L_s=120-140^\circ$ period, which corresponds to northern hemisphere (NH) summer. The zonally averaged temperatures are relatively uniform within the 40°S to 40°N latitude band and the coldest temperatures are found in the southern (winter) hemisphere. The pattern of cold morning temperatures over the Tharsis plateau ($\sim 250^\circ\text{E}$) is a robust feature in the TES data for all seasons examined ($L_s=108$ to 350°) and is also present in Viking IRTM data.

An approximation of the diurnal-mean field may be constructed by forming $T_{avg} = (T_{pm} + T_{am})/2$. This formulation misses potential contributions from the higher order, even harmonics ($\sigma=2,4,\dots$). Stationary waves, which are the deviations from the zonal mean of T_{avg} , are shown in Fig. 1c. The stationary wave field is largely confined to latitudes where the meridional temperature gradient indicates the presence of strong westerly flow and is dominated by zonal wave 1 with additional wave 2 and 3 components. There is a slow evolution in the structure and amplitude of the SH stationary wave pattern over the $L_s=108-220^\circ$ period and a comparable wave pattern emerges in the NH later in the season ($L_s\sim 175^\circ$) as westerly zonal winds continue to develop in response to the cooling north polar temperatures.

Similarly, a diurnally-varying (tide) field can be formulated as $T_{tide} = (T_{pm} - T_{am})/2$ as shown in Fig. 1d. Note that T_{tide} has both a zonally-uniform component associated with the migrating (sun-synchronous) tide and zonal structure due to the presence of nonmigrating tide components. The migrating tide is likely significantly aliased in midlatitudes as the expected diurnal temperature range for this component is largest for 6 pm-6 am [Wilson and Richardson, 2000]. The tides are notably more prominent than stationary waves in the 30°S to 30°N latitude range. The top panels in Fig. 2 display the wave 2 and 3 (nonmigrating) components of T_{tide} . The general pattern shows little variation with season. The broad meridional response with relatively little phase variation suggests the presence of Kelvin waves. Of course, the sampling of only 2 local times precludes distinguishing diurnal harmonics from, say, semidiurnal harmonics, or isolating the westward and eastward propagating components.

4. MGCM Tide Simulation

In order to gain insight into the interpretation of the waves in the TES data, we turn to an examination of zonal temperature variations in an MGCM simulation of the NH summer season. The GFDL MGCM is described in WH96 and is formulated with 40 model levels extending to 90 km and incorporates MOLA topography [Smith *et al.*, 1999]. Good agreement with the TES zonal-mean temperatures is obtained with a dust distribution that is concentrated in tropical latitudes with a relatively low column opacity. The simulated stationary wave field (not shown) is quite similar to the observed wave. The wave 2 and 3 components of the simulated T_{tide} field, shown in the bottom panels of Fig. 2, can be seen to compare favorably with the observed waves. In particular, the

phases are in very good agreement. The simulated wave 1 tide component (not shown) also compares well with corresponding observed field.

The diurnal variation of simulated equatorial T_{15} is shown in Fig. 3a. The tide response is particularly strong in the vicinity of Tharsis, while the zonally-averaged diurnal variation (the sun-synchronous tide) is relatively weak, as discussed in *Wilson and Richardson [2000]*. The zonal wave 2 and 3 variations, shown in Figs. 3b and 3c, respectively, indicate the prominent presence of eastward propagating wave components. In each case, the temporal variation is dominated by the diurnal harmonic with only weak contributions from higher harmonics. The simulated wave 2 field also includes a small stationary wave contribution. The wave 2 variation is largely the result of an eastward propagating zonal wave 1 and a somewhat weaker westward zonal wave 3, as is consistent with the discussion in Section 2. Similarly, the wave 3 variation is due to an eastward, zonal wave 2 and a westward, zonal wave 4. The wave 1 component of the equatorial T_{15} response (not shown) appears as a diurnal period standing wave which is consistent with a zonally-symmetric diurnal tide ($s=0$, $\sigma=1$) as viewed in a fixed local time reference.

Figure 4 shows that the amplitudes of the diurnal period, eastward propagating components ($T_{-1,1}$, $T_{-2,1}$, $T_{-3,1}$) derived from the simulated zonal wave 2, 3 and 4 temperature variations generally correspond to the theoretically expected meridional structure of DK1, DK2 and DK3, respectively. The eastward propagating tides appear to be consistent with diurnal Kelvin waves.

It should be emphasized that the relative mix of eastward and westward propagating tides is dependent on the vertical weighting of the temperature field. An examination of the diurnal variation of the simulated 3-D temperature field reveals considerable small scale horizontal and vertical structure, representing a rich mix of eastward and westward propagating tides, particularly in the tropics. Eastward propagating waves are prominent in the present analysis due to their deep vertical structure relative to the westward propagating waves, which tend to be smoothed by the use of the IRTM vertical weighting function. Geopotential represents a vertical integration of temperature so that waves with relatively coherent vertical structure are enhanced. The result is that simulated geopotential fields are found to generally reflect the expected vertical and meridional structure of diurnal Kelvin waves. For example, Fig. 5 shows that the wave 2 equatorial geopotential field has the barotropic vertical structure corresponding to DK1 and the wave 3 field has a long vertical wavelength consistent with DK2 as discussed in Section 2.

Discussion

The presence of eastward propagating waves in the MGCM simulation and the meridional structure of the observed temperature structures (Fig. 2) suggest that the tide modes in the TES T_{15} data may be identified, in large part, as diurnal period Kelvin waves. The propagation of these waves to thermospheric heights suggests an explanation for the prominent wave 2 and 3 variations in atmospheric density at 130 km that have been inferred from MGS accelerometer data obtained during the two phases of aerobraking [*Keating et al.*, 1998,

2000; *Forbes and Hagan*, 2000]. Significantly, the phase and meridional structure of the wave 2 temperature variation in Fig. 2 are in close agreement with the observed wave 2 density structure in the accelerometer data [Keating et al., 2000] collected during NH spring ($L_s=35-87^\circ$). The phases of the nonmigrating tides in the TES data show little variation with season so that this comparison is warranted. The phase of the simulated (and observed) DK1 variation in T_{15} also matches the phase of the DK1 inferred from the record of surface pressure observations at the two Viking lander sites [WH96]. We thus find that the presence of a barotropic DK1 in the Mars atmosphere provides a reasonable description of the observed wave 2 TES T_{15} temperature variation and is also consistent with the signature of the DK1 in Viking surface pressure data and in MGS accelerometer data at 130 km.

Acknowledgements. The author would like to thank Josh Bandfield for synthesizing T_{15} temperatures from the TES spectra. This work was supported by a grant from the NASA Mars Data Analysis program.

References

- Banfield, D., B. Conrath, J.C. Pearl, and M.D. Smith, Thermal tides and stationary waves on Mars as revealed by Mars Global Surveyor Thermal Emission Spectrometer, *J. Geophys. Res.*, *105*, 9521-9537, 2000.
- Chapman, S. and R.S. Lindzen, *Atmospheric Tides*, 201 pp., D. Reidel, Norwell, MA, 1970.
- Conrath, B.J., Influence of planetary-scale topography on the diurnal thermal tide during the 1971 martian dust storm, *J. Atmos. Sci.*, *33*, 2430-2439, 1976.
- Conrath, B. J., J. C. Pearl, M. D. Smith, W. C. Maguire, P. R. Christensen, S. Dason, and M.S. Kaelberer, Mars Global Surveyor Thermal Emission Spectrometer (TES) observations: Atmospheric temperatures during aerobraking and science phasing, *J. Geophys. Res.*, *105*, 9509-9519, 1999.
- Forbes, J.M., and M.E. Hagan, Diurnal Kelvin wave in the atmosphere of Mars: Towards an understanding of 'stationary' density structures observed by the MGS accelerometer, *Geophys. Res. Lett.*, *in press*, 2000.
- Keating, G.M. et al., The structure of the upper atmosphere of Mars: in-situ accelerometer measurements from Mars Global Surveyor, *Science*, *279*, 1672-1676, 1998.
- Keating, G.M. et al., Evidence for large global diurnal Kelvin wave in the Mars upper atmosphere, abstract 50:02, *Bull. Am. Astron. Soc.*, *32*, 2000.
- Smith D.E., et al., The global topography of Mars and implications for surface evolution, *Science*, *284*, 1495-1503, 1999.
- Wilson, R.J., and K. Hamilton, Comprehensive model simulation of thermal tides in the martian atmosphere, *J. Atmos. Sci.*, *53*, 1290-1326, 1996.
- Wilson, R.J., and M.I. Richardson, The martian atmosphere during the Viking mission, 1: Infrared measurements of atmospheric temperatures revisited, *Icarus*, *145*, 555-579, 2000.
- Zurek, R.W., Diurnal tide in the martian atmosphere, *J. Atmos. Sci.*, *33*, 321-337, 1976.
- Zurek, R.W., Free and forced modes in the martian atmosphere, *J. Geophys. Res.*, *93*, 9452-9462, 1988.

(Received July 11, 2000; revised August 31, 2000;
accepted September 9, 2000.)

Figure Captions

Figure 1. TES T_{15} temperatures binned into 5 degree latitude and longitude boxes. (a) 2 am temperatures. (b) 2 pm temperatures. (c) Stationary wave field given by deviations from the zonal mean of $(T_{pm} + T_{am})/2$. (d) Tide field, T_{tide} , given by $(T_{pm} - T_{am})/2$.

Figure 2. (a) Zonal wave 2 component of the TES T_{tide} of Fig. 1d. (b) Zonal wave 3 component of TES T_{tide} . (c) Zonal wave 2 component of simulated T_{tide} . (d) Zonal wave 3 component of simulated T_{tide} . The contour increment is 0.5 K.

Figure 3. (a) Diurnal variation of simulated equatorial (10°S - 10°N) T_{15} . Shading indicates negative deviations from the local diurnal mean temperature. (b) Zonal wave 2 component. Arrows indicate eastward (solid, $T_{-1,1}$) and westward (dashed, $T_{3,1}$) wave propagation. (c) Zonal wave 3 component, composed of eastward, $T_{-2,1}$ and westward, $T_{4,1}$ waves. The contour interval for panels b and c is 0.5 K.

Figure 4. Amplitudes of the diurnal period, eastward propagating components derived from the simulated zonal wave 2, 3 and 4 temperature variations ($T_{-1,1}$, $T_{-2,1}$, $T_{-3,1}$ respectively). The $s=-1$ and $s=-2$ curves have been offset by 2 K and 1 K, respectively. The grey curves indicate the expected meridional structure for the diurnal Kelvin waves (DK1, DK2 and DK3).

Figure 5. Longitude-height sections of equatorial 2 pm geopotential for simulated (a) zonal wave 2 and (b) zonal wave 3. The contour interval is 100 meters.

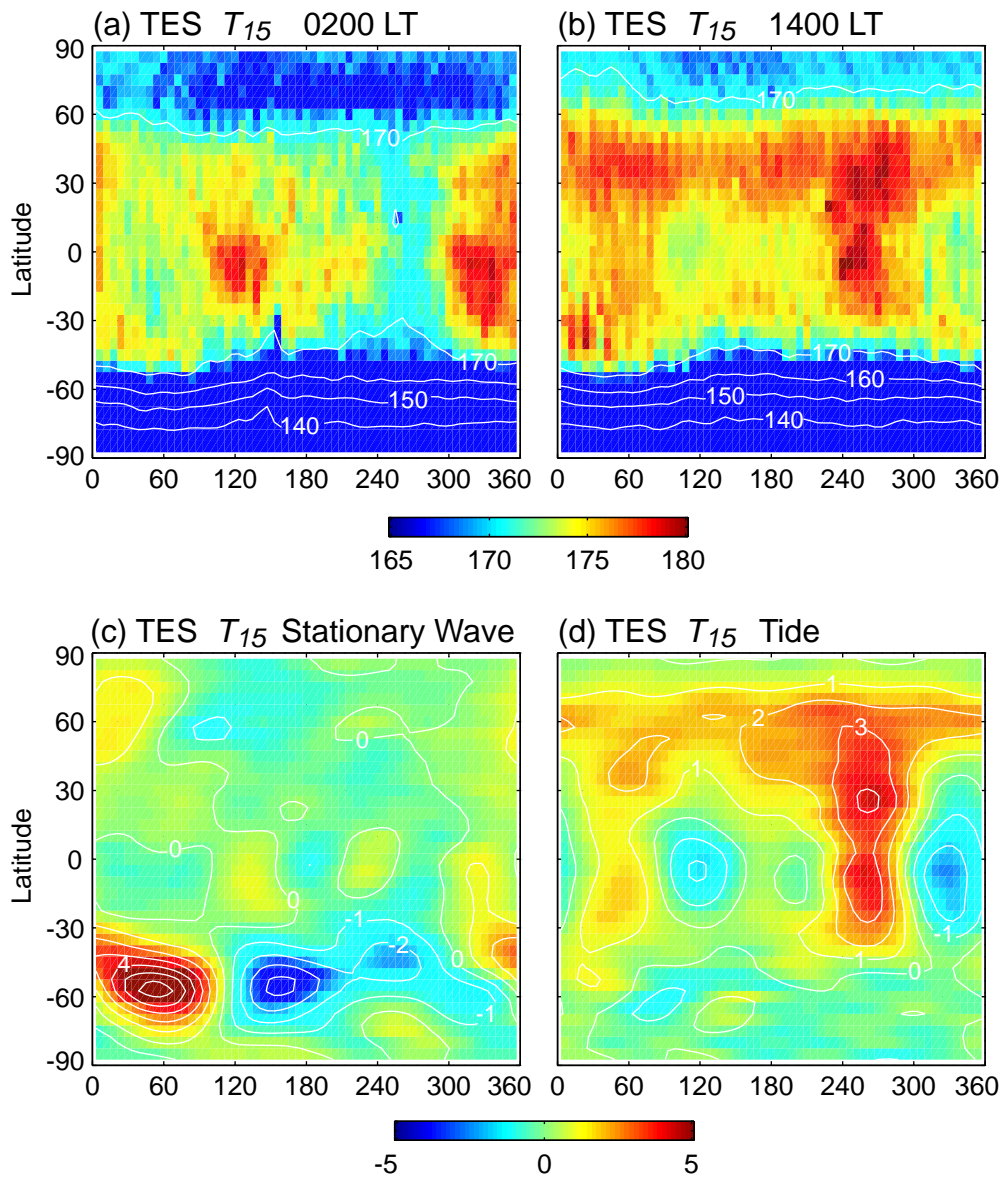


Figure 1. TES T_{15} temperatures binned into 5 degree latitude and longitude boxes. (a) 2 am temperatures. (b) 2 pm temperatures. (c) Stationary wave field given by deviations from the zonal mean of $(T_{pm} + T_{am})/2$. (d) Tide field, T_{tide} , given by $(T_{pm} - T_{am})/2$.

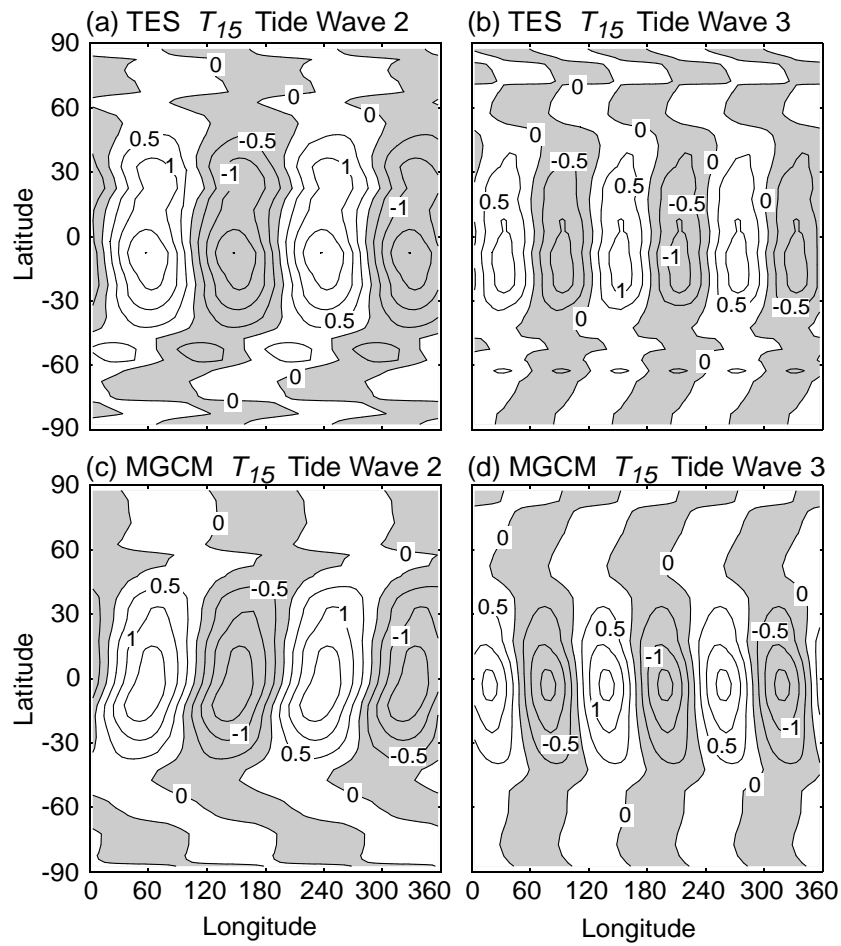


Figure 2. (a) Zonal wave 2 component of the TES T_{tide} of Fig. 1d. (b) Zonal wave 3 component of TES T_{tide} . (c) Zonal wave 2 component of simulated T_{tide} . (d) Zonal wave 3 component of simulated T_{tide} . The contour increment is 0.5 K.

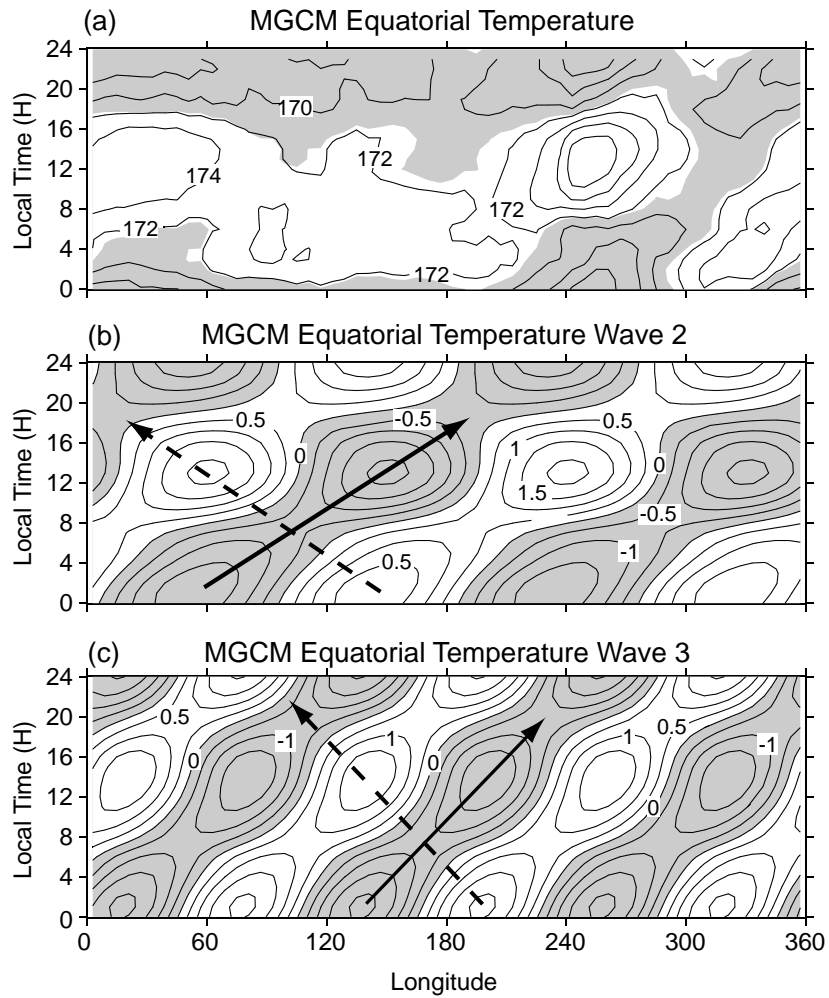


Figure 3. (a) Diurnal variation of simulated equatorial (10°S - 10°N) T_{15} . Shading indicates negative deviations from the local diurnal mean temperature. (b) Zonal wave 2 component. Arrows indicate eastward (solid, $T_{-1,1}$) and westward (dashed, $T_{3,1}$) wave propagation. (c) Zonal wave 3 component, composed of eastward, $T_{2,1}$ and westward, $T_{4,1}$ waves. The contour interval for panels b and c is 0.5 K.

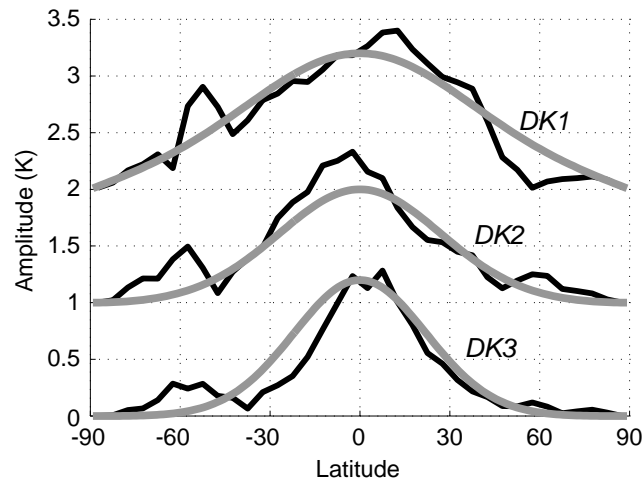


Figure 4. Amplitudes of the diurnal period, eastward propagating components derived from the simulated zonal wave 2, 3 and 4 temperature variations ($T_{-1,1}$, $T_{-2,1}$, $T_{-3,1}$ respectively). The $s=-1$ and $s=-2$ curves have been offset by 2 K and 1 K, respectively. The grey curves indicate the expected meridional structure for the diurnal Kelvin waves (DK1, DK2 and DK3).

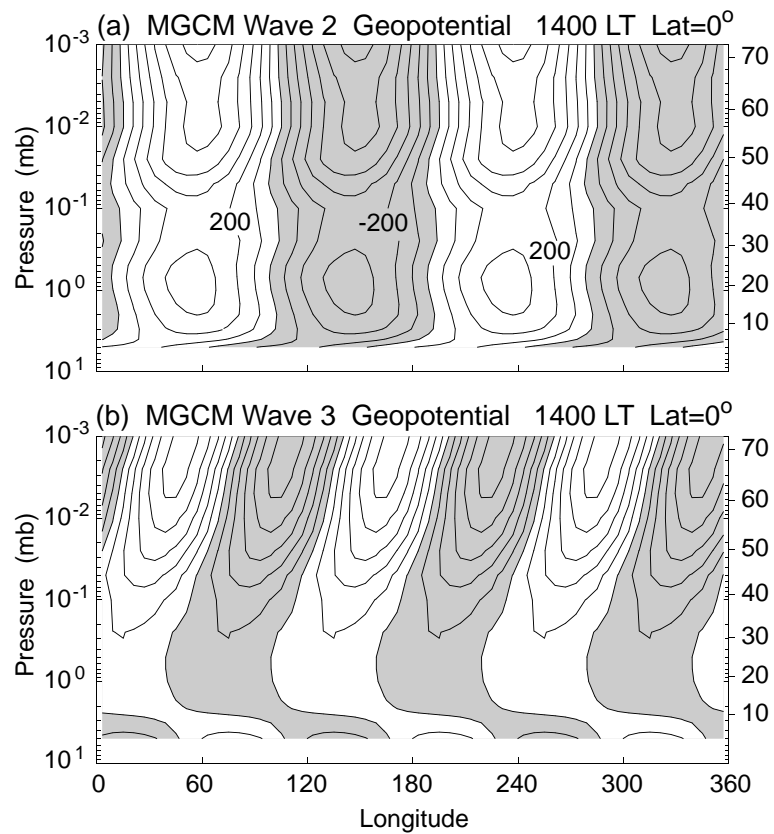


Figure 5. Longitude-height sections of equatorial 2 pm geopotential for simulated (a) zonal wave 2 and (b) zonal wave 3. The contour interval is 100 meters.